Ultrasensitive Assay of Alkaline Phosphatase Based on the Fluorescent Response Difference of the Metal-Organic Framework Sensor

Xi-Yuan Yao et al.

Citation of published version:
Yao, X.-Y., Wang, Q., Liu, Q., Pang, M., Du, X.-M., Zhao, B., Li, Y., & Ruan, W.-J. (2019). Ultrasensitive Assay of Alkaline Phosphatase Based on the Fluorescent Response Difference of the Metal–Organic Framework Sensor. In ACS Omega (Vol. 5, Issue 1, pp. 712–717). American Chemical Society (ACS).
https://doi.org/10.1021/acsomega.9b03337

ACS OMEGA

Article

Cite This: ACS Omega 2020, 5, 712−717

http://pubs.acs.org/journal/acsodf

Ultrasensitive Assay of Alkaline Phosphatase Based on the Fluorescent Response Difference of the Metal−Organic Framework Sensor

Xi-Yuan Yao,[†,‡] Qian Wang,[†] Qiao Liu,[†] Meili Pang,[†] Xiao-Meng Du,[†] Bo Zhao,[†] Yue Li,*[,†,§] and Wen-Juan Ruan*[,†,§]

[†]College of Chemistry, Nankai University, No. 94 of Weijin Road, Tianjin 300071, China

[‡]Department of Chemistry and Biochemistry, The University of Alabama, Tuscaloosa, Alabama 35487, United States

[§]Key Laboratory of Advanced Energy Materials Chemistry (Ministry of Education), Nankai University, Tianjin 300071, China

Supporting Information

ABSTRACT: The assay of alkaline phosphatase (ALP) is important in clinical diagnosis because the abnormal expression of this enzyme is related to many serious diseases. In this work, using a luminescent metal−organic framework (MOF) as the sensor, a fluorescent method was developed for the activity assay of ALP. With nanoscale particle size, the prepared MOF sensor exhibited good dispersability and stable photoluminescence in aqueous suspension. The emission of this MOF is inert to *p*-nitrophenylphosphate (NPP) but could be efficiently quenched by its dephosphorylated product, *p*-nitrophenol. Taking advantage of this feature, this MOF was added to the system of ALP-catalyzed NPP dephosphorylation to transduce the proceeding of the reaction real-timely to the fluorescent signal. The enzyme activity could be calculated based on the recorded kinetic trace. This method presented a low detection limit (2×10^{-3} U L^{-1}) and a wide quantification range (0.6−90 U L^{-1}) in our experiments, showing its quantification capability challenges the best of current ALP analytical methods. As a practical application, our method was successfully applied to the ALP analysis in human serum samples.

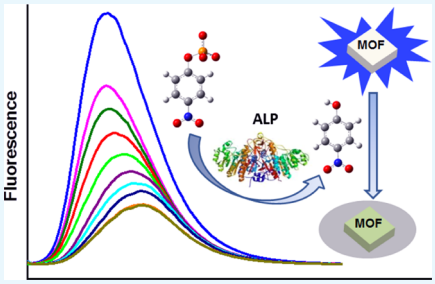

INTRODUCTION

Alkaline phosphatases (ALPs) are a group of isoenzymes that catalyze hydrolysis and transphosphorylation of monophosphates. This kind of enzymes distribute widely in mammalian tissues and participate in a series of important physiological processes.[1] Clinically, serum ALP activity is routinely used as a diagnostic biomarker for several serious diseases, including breast and prostatic cancers,[2,3] bone disease,[4] liver dysfunction,[5] and diabetes.[6] Because of its importance, various methods have been proposed for the activity measurement of ALP.[7−12] Among these methods, fluorometric assay shows great potential because of its intrinsic advantages in sensitivity, operability, and instrument requiring. Until now, different kinds of fluorescent sensors, including organic molecules[8,9] and inorganic nanomaterials,[10−12] have been applied to the activity assay of ALP.

As a novel kind of inorganic-organic hybrid materials, metal−organic frameworks (MOFs) have shown great potential in fluorescent sensing during the past decade.[13] Besides structural flexibility and porosity, MOFs also present low cytotoxicity and biodegradability, which makes these kinds of materials extremely suitable for biological analysis, particularly for the enzyme assay.[14] With different responses to the substrate and the product, the MOF sensor could transduce the proceeding of enzymatic reaction to fluorescent signal real-timely. Recently, several research groups, including ours, have developed a number of successful MOF-based sensing systems for the activity measurement of different kinds of enzymes.[15−17] These systems usually exhibit high sensitivity and can distinguish the target enzymes from a series of interfering species.

In this work, a luminescent MOF (In-atp) with particle size in the nanoscale was synthesized. The study about the fluorescent response of this material showed that its emission is insusceptible to monophosphate but could be efficiently quenched by the hydrolysis product. With this response difference, this MOF was successfully applied to the activity assay of ALP.

RESULTS AND DISCUSSION

Characterization of In-atp. In-atp was obtained as white powder from the reaction between deprotonated 2-aminoterephthalic acid (H_2atp) and $InCl_3$ in the mixed solvent of dimethylformamide (DMF)/H_2O (v/v = 4/1, Figure 1a). The coordination structure of the product was characterized by powder X-ray diffraction (PXRD). Well-defined diffraction peaks recorded in the pattern shows the good crystallinity of the sample (Figure 1b). The positions of these peaks are

Received: October 8, 2019
Accepted: December 18, 2019
Published: December 31, 2019

DOI: 10.1021/acsomega.9b03337
ACS Omega 2020, 5, 712−717

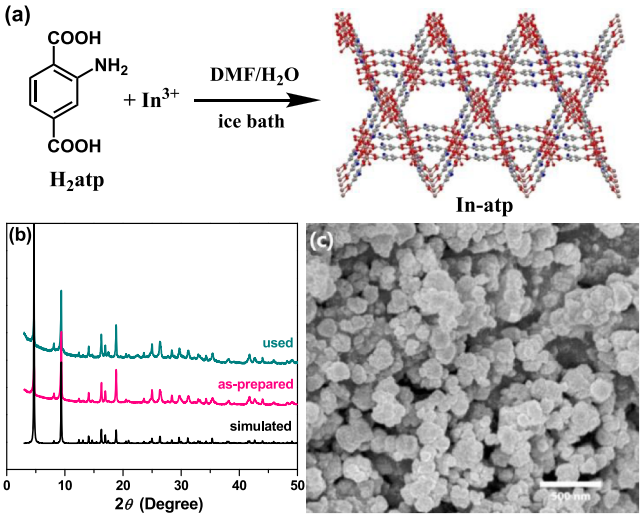

Figure 1. (a) Schematic illustration of the synthetic process, (b) PXRD pattern, and (c) SEM image of In-atp.

consistent with the simulated pattern from the In analogue of MIL-68 (constructed with the ligand of terephthalic acid),[18] indicating that our sample is isostructural with it. In the Fourier transform infrared spectrum (Figure S1), the carboxyl groups give doublet peaks at 1556 and 1425 cm^{-1}, while no characteristic absorption band is observed in the range of 1690−1730 cm^{-1}, indicating the complete deprotonation of H_2atp upon the construction of In-atp. Elemental and thermogravimetric analyses (Figure S2) of In-atp gave the empirical formula of $[In(atp)(OH)]\cdot 0.5H_2O$. These results further confirm the network structure determined by PXRD. In this framework, the carboxyl groups of atp^{2-} ligands coordinate with In^{3+} ions to construct the backbone of MOFs, while their amino groups are left free to work as auxochromes. The residual coordination sites of In^{3+} are saturated by OH^- ions. Scanning electron microscopy (SEM) observation showed that the obtained sample is composed of irregular shaped particles with size in the range of 100−200 nm (Figure 1c). This small particle size is good for the dispersability of MOF in the suspension.

Photoluminescence Property and Response. With fluorescent atp^{2-} as the ligand and closed-shell In^{3+} as the metal node, In-atp is promising in terms of photoactivity. The photoluminescence of In-atp was directly examined with its aqueous suspension (to be the same as the following enzyme assay experiments, Tris-HCl buffer was added to maintain the pH at 8.0). As expected, In-atp gave a ligand-centered fluorescence band with the maximum at 429 nm (Figure 2a). The emission intensity of the MOF is nearly three times higher than that of the free H_2atp ligand. However, the fluorescence quantum yield of In-atp (44.3%) did not show such high increase extent (32.0% for H_2atp). The suspension exhibited good stability under experimental conditions. Placed in the cuvette of fluorescence measurement, its emission showed no noticeable change in 30 min (Figure S3), which is long enough for normal kinetic measurements. We also tested the effect of medium pH on the fluorescence spectrum and observed that the emission intensity of In-atp gave a plateau in the pH range of 7−11 (Figure S4). This range covers the optimal pHs of the ALPs from different origins (8−10),[19−21] illustrating the suitability of In-atp for the analysis of this kind of enzyme.

We selected *p*-nitrophenylphosphate (NPP), which is commonly used in the colorimetric assay of ALP, as the substrate for enzymatic reaction. First, we tested the fluorescent responses of In-atp to this compound and its dephosphorylated product, *p*-nitrophenol (NP) (Figures 2b and S5). It was observed that, although both NPP and NP could induce the fluorescence weakening of In-atp, the quenching efficiency of NP is much higher than that of the

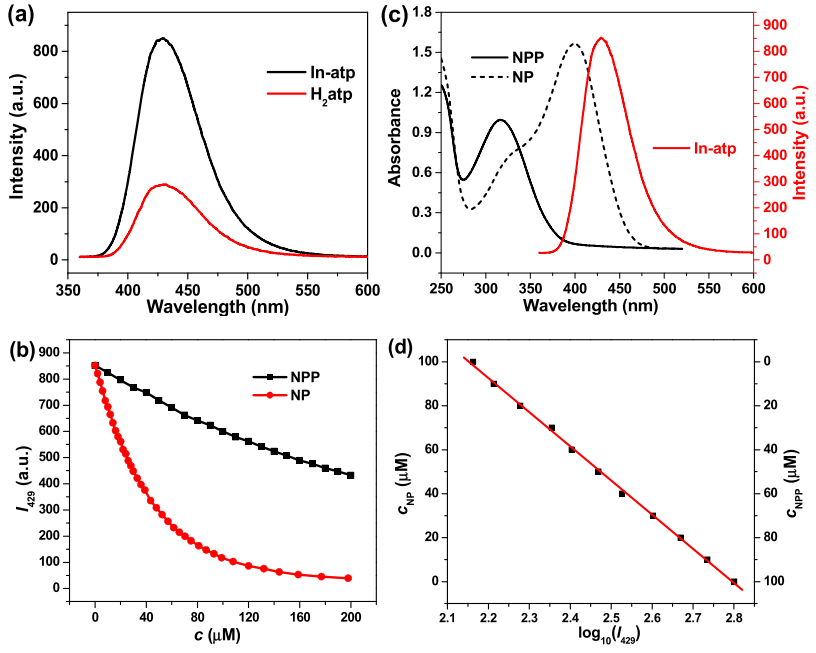

Figure 2. (a) Fluorescence spectra of In-atp and H_2-atp in Tris-HCl buffer (20 mM, pH = 8.0), 50 mg L^{-1} In-atp or H_2-atp, λ_{ex} = 348 nm. (b) Emission intensities of In-atp suspension upon the addition of different amounts of NPP and NP. 50 mg L^{-1} In-atp, λ_{ex} = 348 nm and λ_{em} = 429 nm. (c) Comparison between the emission spectrum of In-atp and the absorption spectra of NPP and NP. (d) Calibration curve of the logarithm of fluorescence intensity versus reaction extent, $c_{NPP} + c_{NP} = 100\ \mu M$.

DOI: 10.1021/acsomega.9b03337
ACS Omega 2020, 5, 712−717

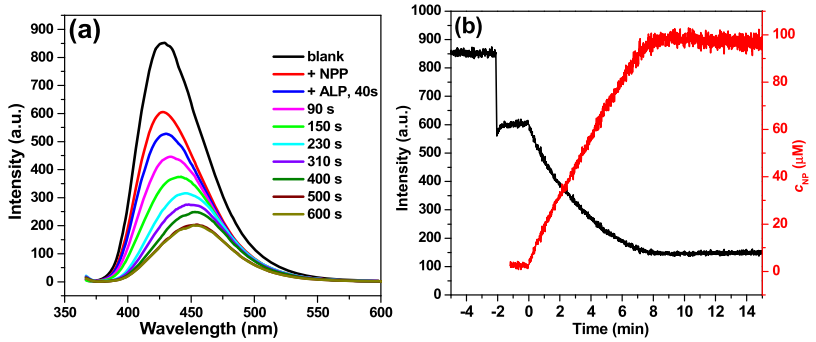

Figure 3. (a) Change of the fluorescence spectrum of In-atp in the ALP-catalyzed dephosphorylation system of NPP. (b) Temporal change of In-atp emission intensity (λ_{em} = 429 nm) and the kinetic curve of the reaction. 50 mg L^{-1} In-atp, c^0_{NPP} = 100 μM and 4 mg L^{-1} ALP, in 3 mL Tris-HCl buffer (20 mM, pH = 8.0).

substrate. For example, the emission of In-atp was nearly completely quenched (87%) upon the addition of 100 μM NP, while the same amount of NPP can only induce a small quenching percentage of 22%. We attribute the higher quenching efficiency of NP to a resonance energy transfer mechanism because the absorption of NPP exhibits a large redshift upon dephosphorylation. As shown in Figure 2c, in contrast to the substrate, the absorption spectrum of NP (with the maximum at 399 nm and extending to 490 nm) overlaps much with the emission band of In-atp, so both Förster resonance energy transfer (FRET) and inner filter effect (IFE) are possible to happen in this sensing system. We used the equation proposed by Parker to evaluate the contributions of these two processes.[22,23]

$$\frac{I_{cor}}{I_{obsd}} = \frac{2.3dA_{ex}}{1 - 10^{-dA_{ex}}} \times 10^{gA_{em}} \times \frac{2.3sA_{em}}{1 - 10^{-dA_{em}}} \quad (1)$$

In this equation, I_{obsd} is the observed intensity, I_{cor} is the corrected intensity deducting IEF, A_{ex} and A_{em} are respectively the quencher absorbances at the excitation and emission wavelengths, and d (1 cm), g (0.4 cm), and s (0.1 cm) are the parameters depending upon the geometry of the measurement. As shown in Figure S6, I_{cor} is located between I_{obsd} and original intensity, showing that both two mechanisms contribute to the quenching process. Based on the position of the I_{cor} plot, we estimated that ~40% of the observed fluorescent quenching is induced by FRET and the remaining 60% is caused by IEF.

It is noteworthy that the fluorescent measurements were carried out at pH = 8.0 and the pK_a of NP is 7.15, which means that NP would be deprotonated in the suspension. As discussed above, the framework of In-atp is rich of coordinating OH^- ions, which provides potential protonation sites to make the MOFs positively charged. This deduction was confirmed by the dynamic light scattering measurement of In-atp suspension, which gave a positive zeta potential of 25.6 mV. With opposite charges, electrostatic attraction would exist between the MOF backbone and NP, and this effect would induce the enrichment of NP. Adsorption experiments confirmed this anticipation (Figure S7). In the concentration range of 0−130 μM (covering the range used in enzyme assays), the adsorption amount of NP is proportional to its equilibrium concentration. Based on this adsorption isotherm and the structure of In-atp, we calculated that the local concentration of NP could reach 358 times higher than its concentration in equilibrium solution. Because the FRET efficiency is dependent on the distance between the donor and the acceptor, this high enrichment ratio greatly enhances the response sensitivity.

Activity Assay of ALP. Because the ALP-catalyzed dephosphorylation of NPP is quantitative and releases the product with higher quenching efficiency, it is expected that, if In-atp were added to the reaction system, its emission would weaken with the proceeding of the reaction. Because the quenching percentages of NPP and NP showed the biggest difference at 100 μM (Figure 2b), we chose it as the initial concentration of NPP to maximize the fluorescence change. Considering that the formed PO_4^{3-} ion during the enzymatic reaction could potentially induce the decomposition of MOFs, we evaluated the stability of In-atp in the aqueous solutions with different PO_4^{3-} concentrations. As shown in Figure S8, the immersed In-atp maintained its crystallinity when the PO_4^{3-} concentration was below 200 μM. Therefore, at 100 μM of initial substrate concentration, the formed PO_4^{3-} cannot induce the collapse of the MOF sensor. With the addition of 4 mg L^{-1} ALP, the emission of In-atp presented a continuous quenching in the first 500 s and then leveled off, indicating that the dephosphorylation had gone to completion (Figure 3a). The PXRD pattern of the used sensor showed that its structure was unchanged (Figure 1b). We also tested the response speeds of In-atp to NPP and NP. In these experiments, the emission intensities of MOFs were immediately decreased to a steady value after the addition of these compounds (Figure S9), which indicates that the responses of In-atp to NPP and NP are fast enough to follow the enzymatic reaction. The observed temporal change of In-atp emission in the reaction system could be treated as a signal to reflect the kinetics of dephosphorylation.

To determine the reaction rate, we still need the correlation between reaction extent and fluorescence intensity. Because the total amount of NPP and NP was unchanged during enzymatic dephosphorylation, to simulate the reaction media, we prepared a series of NPP−NP mixed solutions with the total concentration of 100 μM but different relative ratios and recorded the fluorescence spectra of In-atp in these solutions (Figure S10). It was observed that the logarithm of fluorescence intensity showed a good linear relationship (R^2 = 0.9989) with the concentrations of NP and NPP (Figure 2d). The calibration curve could be presented as

$$c_{NP} = 100 - c_{NPP} = -155.4 \times \log_{10}(I_{429}) + 434.6 \quad (2)$$

Considering that the relative measurement error of fluorescent intensity was about 0.4%, this equation means that even 0.8 μM of reaction could be reflected as a remarkable

DOI: 10.1021/acsomega.9b03337
ACS Omega 2020, 5, 712−717

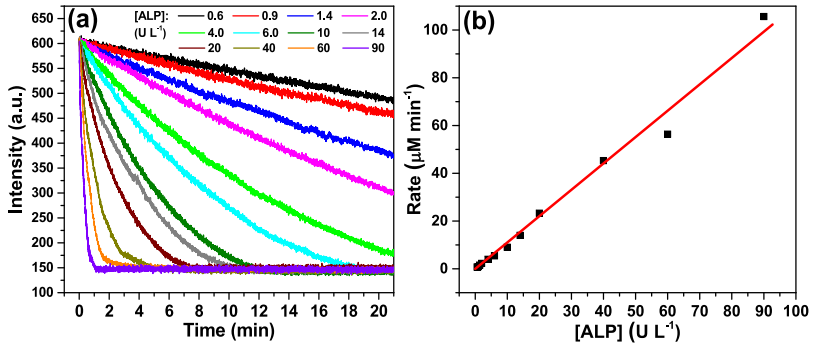

Figure 4. (a) Fluorescence monitoring of NPP dephosphorylation catalyzed by different concentrations of ALP. 50 mg L^{-1} In-atp, c^0_{NPP} = 100 μM, in 3 mL Tris-HCl buffer (20 mM, pH = 8.0). (b) Reaction rates measured at different ALP concentrations.

fluorescent signal (at 3σ level). With this equation, the recorded fluorescence decay curve could be transduced to the kinetic trace of the enzymatic reaction (Figure 3b). By the fitting of the data points in the linear part of the reaction (R^2 = 0.9884), the initial reaction rate was calculated to be 14 μM min^{-1}. Thus, the activity of ALP in the reaction system was 14 U L^{-1}.

The accuracy and sensitivity of this assay were evaluated by the kinetic measurements of the reactions catalyzed by different concentrations of ALP [0.17–26 mg L^{-1} (0.6–90 U L^{-1}), Figure 4a]. The measured initial reaction rates presented a strict proportional relationship with enzyme amounts (R^2 = 0.9907, Figure 4b), proving that our method can precisely reflect the activity of ALP. With the slope of this fitting line and the measurement error of the reaction rate, the detection limit for ALP was calculated to be 2 × 10^{-3} U L^{-1} (3σ/k), showing that the sensitivity of this system is superior to most of the recently reported spectroscopic ALP assay methods (see Table S1 for a literature survey). It should be noted that the serum ALP levels in adults are generally in the range of 40–190 U L^{-1}. Even considering the dilution and pH modulation processes of raw serum samples before measurement, the wide quantification range and high sensitivity of our method is still sufficient for clinical diagnosis. Additionally, although several MOF-based spectroscopic methods have been reported for the activity assay of ALP, yet all of these systems used phosphate and/or pyrophosphate ion as the mediator.[24−27] The widespread presence of these two species in biological samples makes these methods susceptible to the matrix effect in practical analysis. Our method does not suffer from this problem because neither the substrate NPP nor the product NP is a natural metabolite.

Encouraged by the above results, we further applied In-atp to the analysis of real serum samples. The standard addition method was used in this part of experiments to evaluate the accuracy. Three serum samples were collected from healthy people. Considering that the quantification range of our method is 0.6–90 U L^{-1} and the normal serum ALP level is 40–190 U L^{-1}, these samples were diluted with Tris-HCl buffer by 50 times before measurement. This dilution process also alleviated the effect of serum on the fluorescence of In-atp (probably due to the components with UV–vis absorption) to a negligible level. Although the fluorescence of In-atp in pure serum was much weakened, its emission in 50-fold diluted sample could reach 93% of the intensity in pure Tris-HCl buffer (Figure S11). After the spiking of a certain volume of standard enzyme solution, these samples were measured by In-atp. At three different ALP levels, the relative standard deviations of the repeated measurements (n = 3) were below 8% and the average recoveries were in the range of 95.6–102.9%, showing that In-atp is suitable to analyze these kinds of samples (Table 1).

Table 1. Analytical Results of ALP in Serum Samples

sample	added (U L^{-1})	found (U L^{-1})	recovery (%)
1	10	9.6 ± 0.8	95.6
	100	100.0 ± 1.5	100.0
	400	403.6 ± 7.6	100.9
2	10	9.8 ± 0.7	98.2
	100	96.5 ± 4.2	96.5
	400	411.7 ± 3.4	102.9
3	10	9.6 ± 0.3	96.3
	100	101.1 ± 2.4	101.1
	400	398.7 ± 2.5	99.7

CONCLUSIONS

In summary, a fluorescent method was developed for the activity assay of ALP using an atp^{2-} based nanoscale MOF as sensor. Taking advantage of its stable emission in the suspension and different responses to NPP and NP, this MOF sensor could transduce the extent of ALP catalyzed dephosphorylation real-timely to fluorescent signal. By the scan of this signal, we could follow the kinetics of the reaction and thus obtain the activity of the enzyme. A low detection limit of 2 × 10^{-3} U L^{-1} and a wide quantification range of 0.6–90 U L^{-1} were presented by this method, showing its advantage over the current ALP assay systems. The results of this work show the wide potential of MOFs in enzyme assay.

EXPERIMENTAL SECTION

Reagents and Instrumentation. All chemicals were obtained commercially and used as received without further purification. The aqueous suspensions used in fluorescence measurements were prepared with ultrapure water.

PXRD patterns were recorded on a Rigaku D/Max-2500 diffractometer with Cu Kα radiation (λ = 0.15406 nm) and samples were scanned at 60 kV and 300 mA. Elemental compositions (C, H, and N) of samples were measured by using a PerkinElmer 240C analyzer. Thermogravimetric analysis (TGA) was carried out using a Rigaku standard TG-DTA analyzer from ambient temperature to 700 °C with a heating rate of 10 °C min^{-1} in the air, and an empty Al_2O_3 crucible was used as the reference. SEM images were taken by using a JEOL JSM-7500F scanning electron microscope.

DOI: 10.1021/acsomega.9b03337
ACS Omega 2020, 5, 712−717

Steady state fluorescence experiments were carried out on an Agilent G9800A fluorescence spectrometer, and an SPVF-1X0 accessory was used to control the sample temperature at 25 °C. A Rikakikai NTT-2200P accessory was used to control the temperature. Absorption spectra were recorded by using a Shimadzu UV-2450 spectrophotometer. Zeta potential was measured using a ZETAPALS/BI-200SM analyzer.

Synthesis of In-atp. H_2atp (0.045 g) and NaOH (0.22 g) were dissolved in a mixed solvent of H_2O (5 mL) and DMF (40 mL) and placed in ice bath. Then, 5 mL aqueous solution of $InCl_3$ (0.11 g) was added dropwise to it under vigorous stirring. The mixture was stirred for 30 min under cooling and further reacted for 2.5 h at room temperature. The formed yellow precipitate of In-atp was separated by centrifugation, washed with DMF, H_2O, and ethanol in sequence, and dried at 60 °C in air for 12 h. Anal. Calcd. (%) for $[In(atp)(OH)]\cdot 0.5H_2O$ (M_w = 319.97): C, 30.03; H, 2.21; N, 4.38. Found: C, 30.22; H, 2.15; and N, 4.60.

Fluorescent Assay of ALP Activity. The powder of In-atp (25 mg) was immersed in 500 mL Tris-HCl buffer (20 mM, pH = 8.0) which contains $ZnCl_2$ (1 mM) and $MgCl_2$ (1 mM). This mixture was ultrasonicated for 2 h and then left standing for a day to get a stable suspension (50 mg L^{-1}). Suspension (3 mL) was placed in a 1 × 1 cm^2 optical quartz cuvette with continuous stirring at 25 °C. After sequential addition of NPP and ALP, the fluorescence emission of the sample was monitored continually (λ_{ex} = 348 nm, λ_{em} = 429 nm, the excitation and emission slit widths were both set at 1.5 nm).

■ ASSOCIATED CONTENT

Supporting Information

The Supporting Information is available free of charge at https://pubs.acs.org/doi/10.1021/acsomega.9b03337.

Experimental details, TGA curve, temporal emission intensity change of MOF suspension with prolonging placement and NPP/NP addition, fluorescent spectra of In-atp at different pH values and different concentrations of NPP and NP, adsorption of NP on In-atp, and the performance comparison with literatures (PDF)

■ AUTHOR INFORMATION

Corresponding Authors

*E-mail: liyue84@nankai.edu.cn (Y.L.).
*E-mail: wjruan@nankai.edu.cn (W.-J.R.).

ORCID

Wen-Juan Ruan: 0000-0001-5889-1043

Notes

The authors declare no competing financial interest.

■ ACKNOWLEDGMENTS

This work was supported by the NSFC (21673121 and 21876087) and the Research Fund for 111 Project (B12015).

■ REFERENCES

(1) Coleman, J. E. Structure and mechanism of alkaline phosphatase. *Annu. Rev. Biophys. Biomol. Struct.* **1992**, *21*, 441.

(2) Huggins, C.; Hodges, C. V. Studies on prostatic cancer: I. The effect of castration, of estrogen and of androgen injection on serum phosphatases in metastatic carcinoma of the prostate. *Ca-Cancer J. Clin.* **1972**, *22*, 232−240.

(3) Sturgeon, C. M.; Duffy, M. J.; Stenman, U.-H.; Lilja, H.; Brunner, N.; Chan, D. W.; Babaian, R.; Bast, R. C., Jr.; Dowell, B.; Esteva, F. J.; Haglund, C.; Harbeck, N.; Hayes, D. F.; Holten-Andersen, M.; Klee, G. G.; Lamerz, R.; Looijenga, L. H.; Molina, R.; Nielsen, H. J.; Rittenhouse, H.; Semjonow, A.; Shih, I.-M.; Sibley, P.; Soletormos, G.; Stephan, C.; Sokoll, L.; Hoffman, B. R.; Diamandis, E. P. National academy of clinical biochemistry laboratory medicine practice guidelines for use of tumor markers in testicular, prostate, colorectal, breast, and ovarian cancers. *Clin. Chem.* **2008**, *54*, No. E11−E79.

(4) Miller, P. D. Bone disease in CKD: A focus on osteoporosis diagnosis and management. *Am. J. Kidney Dis.* **2014**, *64*, 290−304.

(5) Ooi, K.; Shiraki, K.; Morishita, Y.; Nobori, T. High-molecular intestinal alkaline phosphatase in chronic liver diseases. *J. Clin. Lab. Anal.* **2007**, *21*, 133−139.

(6) Kemink, S. A. G.; Hermus, A. R. M. M.; Swinkels, L. M. J. W.; Lutterman, J. A.; Smals, A. G. H. Osteopenia in insulin-dependent diabetes mellitus; prevalence and aspects of pathophysiology. *J. Endocrinol. Invest.* **2000**, *23*, 295−303.

(7) Koncki, R.; Ogończyk, D.; Głąb, S. Potentiometric assay for acid and alkaline phosphatase. *Anal. Chim. Acta* **2005**, *538*, 257−261.

(8) Kim, T.-I.; Kim, H.; Choi, Y.; Kim, Y. A fluorescent turn-on probe for the detection of alkaline phosphatase activity in living cells. *Chem. Commun.* **2011**, *47*, 9825−9827.

(9) Tan, Y.; Zhang, L.; Man, K. H.; Peltier, R.; Chen, G.; Zhang, H.; Zhou, L.; Wang, F.; Ho, D.; Yao, S. Q.; Hu, Y.; Sun, H. Reaction-based off-on near-infrared fluorescent probe for imaging alkaline phosphatase activity in living cells and mice. *ACS Appl. Mater. Interfaces* **2017**, *9*, 6796−6803.

(10) Choi, Y.; Ho, N.-H.; Tung, C.-H. Sensing phosphatase activity by using gold nanoparticles. *Angew. Chem., Int. Ed.* **2007**, *46*, 707−709.

(11) Li, G.; Fu, H.; Chen, X.; Gong, P.; Chen, G.; Xia, L.; Wang, H.; You, J.; Wu, Y. Facile and sensitive fluorescence sensing of alkaline phosphatase activity with photoluminescent carbon dots based on inner filter effect. *Anal. Chem.* **2016**, *88*, 2720−2726.

(12) Qian, Z. S.; Chai, L. J.; Huang, Y. Y.; Tang, C.; Jia Shen, J.; Chen, J. R.; Feng, H. A real-time fluorescent assay for the detection of alkaline phosphatase activity based on carbon quantum dots. *Biosens. Bioelectron.* **2015**, *68*, 675−680.

(13) Lustig, W. P.; Mukherjee, S.; Rudd, N. D.; Desai, A. V.; Li, J.; Ghosh, S. K. Metal-organic frameworks: Functional luminescent and photonic materials for sensing applications. *Chem. Soc. Rev.* **2017**, *46*, 3242−3285.

(14) Wang, H.-S. Metal−organic frameworks for biosensing and bioimaging applications. *Coord. Chem. Rev.* **2017**, *349*, 139−155.

(15) Song, C.; Wang, G.-Y.; Wang, Y.-L.; Kong, D.-M.; Wang, Y.-J.; Li, Y.; Ruan, W.-J. A barium based coordination polymer for the activity assay of deoxyribonuclease I. *Chem. Commun.* **2014**, *50*, 11177−11180.

(16) Li, Y.; Guo, A.; Chang, L.; Li, W.-J.; Ruan, W.-J. Luminescent metal−organic-framework-based label-free assay of polyphenol oxidase with fluorescent scan. *Chem. - Eur. J.* **2017**, *23*, 6562−6569.

(17) Wang, K.; Li, N.; Zhang, J.; Zhang, Z.; Dang, F. Size-selective QD@MOF core-shell nanocomposites for the highly sensitive monitoring of oxidase activities. *Biosens. Bioelectron.* **2017**, *87*, 339−344.

(18) Volkringer, C.; Meddouri, M.; Loiseau, T.; Guillou, N.; Marrot, J.; Férey, G.; Haouas, M.; Taulelle, F.; Audebrand, N.; Latroche, M. The Kagomé topology of the gallium and indium metal-organic framework types with a MIL-68 structure: Synthesis, XRD, solid-state NMR characterizations, and hydrogen adsorption. *Inorg. Chem.* **2008**, *47*, 11892−11901.

(19) Garen, A.; Levinthal, C. A fine-structure genetic and chemical study of the enzyme alkaline phosphatase of E. Coli I. Purification and characterization of alkaline phosphatase. *Biochim. Biophys. Acta* **1960**, *38*, 470−483.

DOI: 10.1021/acsomega.9b03337
ACS Omega 2020, 5, 712−717

(20) Harada, M.; Udagawa, N.; Fukasawa, K.; Hiraoka, B. Y.; Mogi, M. Inorganic pyrophosphatase activity of purified bovine pulp alkaline phosphatase at physiological pH. *J. Dent. Res.* **1986**, *65*, 125−127.
(21) Lin, J.-M.; Tsuji, A.; Maeda, M. Chemiluminescent flow injection determination of alkaline phosphatase and its applications to enzyme immunoassays. *Anal. Chim. Acta* **1997**, *339*, 139−146.
(22) Parker, C. Measurement of Fluorescence Efficiency. *Photoluminescence of Solutions*; Elsevier: New York 1968; p 261.
(23) Gauthier, T. D.; Shane, E. C.; Guerin, W. F.; Seitz, W. R.; Grant, C. L. Fluorescence quenching method for determining equilibrium constants for polycyclic aromatic hydrocarbons binding to dissolved humic materials. *Environ. Sci. Technol.* **1986**, *20*, 1162−1166.
(24) Ye, K.; Wang, L.; Song, H.; Li, X.; Niu, X. Bifunctional MIL-53(Fe) with pyrophosphate-mediated peroxidase-like activity and oxidation-stimulated fluorescence switching for alkaline phosphatase detection. *J. Mater. Chem. B* **2019**, *7*, 4794−4800.
(25) Hou, L.; Qin, Y.; Li, J.; Qin, S.; Huang, Y.; Lin, T.; Guo, L.; Ye, F.; Zhao, S. A ratiometric multicolor fluorescence biosensor for visual detection of alkaline phosphatase activity via a smartphone. *Biosens. Bioelectron.* **2019**, *143*, 111605.
(26) Wang, C.; Tang, G.; Tan, H. Pyrophosphate ion-triggered competitive displacement of ssDNA from a metal-organic framework and its application in fluorescent sensing of alkaline phosphatase. *J. Mater. Chem. B* **2018**, *6*, 7614−7620.
(27) Wang, C.; Gao, J.; Cao, Y.; Tan, H. Colorimetric logic gate for alkaline phosphatase based on copper(II)-based metal-organic frameworks with peroxidase-like activity. *Anal. Chim. Acta* **2018**, *1004*, 74−81.

DOI: 10.1021/acsomega.9b03337
ACS Omega 2020, 5, 712−717